Mean flow scaling in a spanwise rotating channel

X. I. A. Yang,[1,*] Z.-H. Xia,[2,†] J. Lee,[3] Y. Lv,[4] and J. Yuan[5]

[1]*Mechanical Engineering, Pennsylvania State University, State College, Pennsylvania 16802, USA*
[2]*Department of Engineering Mechanics, Zhejiang University, Hangzhou, Zhejiang 310027, China*
[3]*Aerothermal and Physical Sciences (APS) Department, Raytheon Technologies Research Center, 411 Silver Lane, East Hartford, Connecticut 06108, USA*
[4]*Aerospace Engineering, Mississippi State University, Mississippi State, Mississippi 39759, USA*
[5]*Mechanical Engineering, Michigan State University, East Lansing, Michigan 48824, USA*

(Received 16 January 2020; accepted 16 June 2020; published 7 July 2020)

Since the early work of Johnston [Johnston, Halleent, and Lezius, J. Fluid Mech. **56**, 533 (1972)], the mean flow scaling in a spanwise rotating channel has received much attention. While it is known that the mean velocity near the pressure, turbulent side follows a linear scaling $U = 2\Omega y + C$ at high rotation speeds, the functional dependence of C on the Reynolds number and the rotation number has been an open question. Here, U is the mean velocity, Ω is the constant rotating speed in the spanwise direction, and C is a constant. In this work, we show that $C^+ = \log(l_\Omega^+)/K$, where the superscript $+$ denotes normalization using wall units at the pressure side; $l_\Omega = u_{\tau,p}/2\Omega$ is a rotation-induced length scale; K is a constant and $K \approx \kappa$, where κ is the von Kármán constant; and $u_{\tau,p}$ is the wall friction velocity at the pressure side.

DOI: 10.1103/PhysRevFluids.5.074603

I. INTRODUCTION

Turbulence is often encountered in rotating frames of reference, e.g., over oceans, around windmills, and in turbomachines, where the reference frames in question revolve with the earth and man-made rotating devices [1–4]. The flows are responsible for the transport of water vapor, the generation of lift and drag, and the mixing of fuel and oxidizer in the above contexts. Effects of these flows at practically relevant conditions are difficult to compute accurately by means of direct numerical simulations or wall-resolving large-eddy simulations due to the cost requirement [5], and therefore engineers often have to rely on empirical relations, e.g., the law of the wall, to compute wall friction using velocity information at an off-wall location.

The law of the wall, also referred to as the universal logarithmic law of the wall, was proposed in the early 1930s by Prandtl and von Kármán [6,7]. It asserts that the mean velocity increases linearly with the logarithm of the distance from the wall, i.e., $U^+ = 1/\kappa \log(y^+) + B$, where U is the mean flow velocity at a wall-normal distance y, the superscript $+$ indicates normalization by wall units, κ is the von Kármán constant [8,9], and B is another constant. The logarithmic law of the wall relates wall-shear stresses to velocities at off-wall locations and is useful for wall modeling in a nonrotating reference frame [10–12], but its predictive power is partly lost if the flow is in a rotating device, e.g., in a spanwise rotating channel [13–15].

Figure 1 shows a sketch of a spanwise rotating channel. In addition to the dimensions of the channel, the flow is controlled by two nondimensional numbers, i.e., the rotation number

*xzy48@psu.edu
†0016069@zju.edu.cn

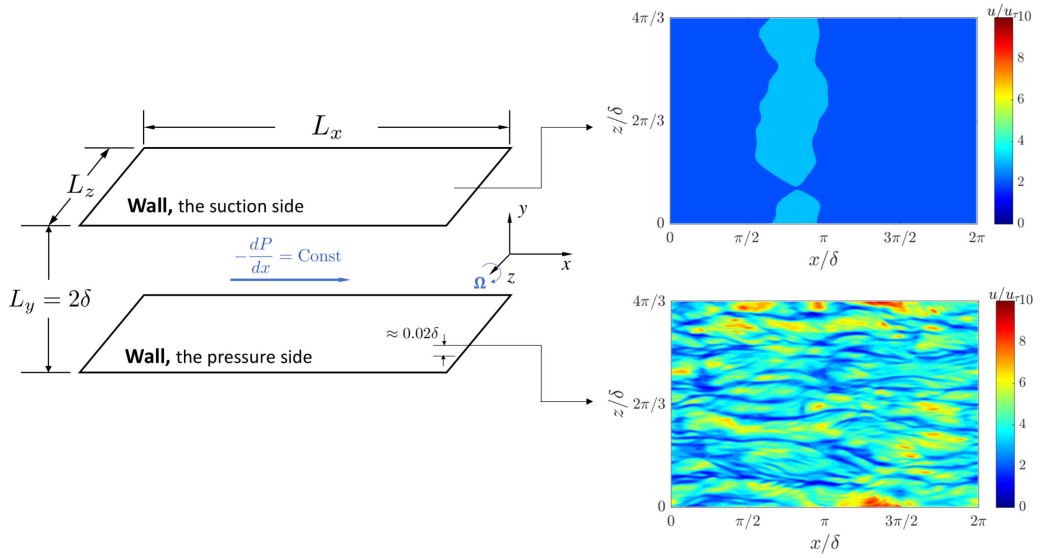

FIG. 1. Left: A sketch of flow in a spanwise rotating channel. Ω is the system rotation speed. x, y, and z are the streamwise, wall-normal, and spanwise directions. In a computational study, a periodic condition is often imposed in the streamwise direction. The domain size is $L_x \times L_y \times L_z$ in the streamwise, wall-normal, and spanwise directions. δ is the half-channel height. Right: Contours of instantaneous streamwise velocities on two x-z planes that are $y/\delta \approx 0.02$ from both walls. The flow near the pressure side remains turbulent, but the flow near the suction side is laminar. The flow is at a global friction Reynolds number $\mathrm{Re}_\tau = 180$ and a friction rotation number $\mathrm{Ro}_\tau = 20$, where u_τ is the global friction velocity. Details of the direct numerical simulation can found in Ref. [17] and the references cited therein.

$\mathrm{Ro}_\tau = 2\Omega\delta/u_\tau$ and the friction Reynolds number $\mathrm{Re}_\tau = u_\tau\delta/\nu$, where Ω is the rotation speed, δ is the half-channel height, ν is the kinematic viscosity, and u_τ is the global friction velocity and is defined as $u_\tau = \sqrt{\delta f_x/\rho}$, with $f_x = -dP/dx$ being the driving body force and ρ being the fluid density. For a spanwise rotating channel, the pressures at the two walls are different due to the Coriolis force, leading to a pressure side and a suction side. We define friction velocities at the two walls and denote them as $u_{\tau,p}$ and $u_{\tau,s}$. These two friction velocities are not necessarily the same and they are related to the global friction velocity as $u_\tau = \sqrt{(u_{\tau,p}^2 + u_{\tau,s}^2)/2}$ [16,17].

Johnston *et al.* [18] showed that, for a channel that rotates about its spanwise axis at a reasonably high speed, the mean flow near the pressure side follows a linear scaling, i.e.,

$$U = 2\Omega y + C, \tag{1}$$

where C is a constant when given Ro_τ and Re_τ. Equation (1) is a counterpart of the conventional universal logarithmic law of the wall, but because the function dependence of C on Ro_τ and Re_τ is not known, Eq. (1) does not have the same predictive power as the universal logarithmic law of the wall.

Since the early work of Johnston *et al.* [18], the scaling of the mean flow has been extensively studied, both experimentally [19–21] and computationally [16,22–24]. Nakabayashi *et al.* [19] conducted dimensional analysis and concluded that the mean velocity at a distance y from the pressure side is a function of the wall-unit-scaled distance from the wall $yu_{\tau,p}/\nu$, the friction Reynolds number Re_τ, and the Coriolis parameter $\mathrm{Rc} = \Omega\nu/u_\tau^2 \equiv \mathrm{Ro}_\tau/2\mathrm{Re}_\tau$. The authors considered data at low rotation numbers ($\mathrm{Ro}_\tau < 0.3$) and low Reynolds numbers ($\mathrm{Re}_\tau < 310$) and argued that system rotation only adds a minor correction to the universal logarithmic law of the wall, where both κ and B may vary as Re_τ and Rc. Later, by analyzing the wind tunnel data from the University

TABLE I. Friction Reynolds numbers and rotation numbers evaluated using quantities at the pressure side for the cases shown in Fig. 2(d). The data may also be found in Ref. [26].

Re_b	$Re_{\tau,p}$	$Ro_{\tau,p}$	Re_b	$Re_{\tau,p}$	$Ro_{\tau,p}$	Re_b	$Re_{\tau,p}$	$Ro_{\tau,p}$	Re_b	$Re_{\tau,p}$	$Ro_{\tau,p}$
5000	130	80.9	10 000	186	112.5	20 000	265	158.3	31 600	670	56.5
5000	144	62.6	10 000	207	86.7	20 000	370	81.0	31 600	988	28.8
5000	170	44.0	10 000	249	60.4	20 000	501	47.8	31 600	1445	9.82
5000	211	28.4	10 000	325	37.0	20 000	677	26.6	31 600	1505	0
5000	258	17.4	10 000	416	21.6	20 000	851	15.3			
5000	310	7.21	10 000	535	8.37	20 000	964	9.29			
5000	326	2.29	10 000	544	0	20 000	1107	2.73			
5000	297	0				20 000	1000	0			

of Melbourne, Nickels and Joubert [25] proposed a rotation correction to the logarithmic law of the wall, i.e., $U^+ = 1/\kappa \ln y^+ + \beta \mathrm{Rc}(y^+ - 35) + 5$, where, $\beta \approx 9.7$ is a constant. However, the dependence of C on Ro and Re remains an open question.

The work addresses this open question. The proposed mean flow scaling is compared to the available direct numerical simulation (DNS) data in the literature [17,26,27]. The data cover a global Reynolds number range from $\mathrm{Re}_\tau = 180$ to about $\mathrm{Re}_\tau \approx 1500$ and a rotation number range from $\mathrm{Ro}_\tau = 0$ to $\mathrm{Ro}_\tau \sim O(100)$. (note that the flow relaminarizes at $\mathrm{Ro}_\tau = \mathrm{Re}_\tau$.) The rest of the paper is organized as follows. We present the mean flow scaling in Sec. II. The arguments that lead to this scaling are presented in Sec. III. Concluding remarks are given in Sec. V following a discussion of the results in Sec. IV.

II. MEAN FLOW SCALING

The flow at the suction side is laminarlike at a high rotation number (see Fig. 1) and the mean flow there is parabolic. We focus on the flow at the pressure side. We define a rotation-induced length scale as follows:

$$l_\Omega = u_{\tau,p}/2\Omega. \tag{2}$$

By definition, $l_\Omega^+ \equiv l_\Omega/(\nu/u_{\tau,p}) = \mathrm{Re}_{\tau,p}/\mathrm{Ro}_{\tau,p}$. From $y = l_\Omega/\kappa$ to $O(\delta)$, the mean flow at the pressure side follows Eq. (1), and the constant C is

$$C^+ \equiv \frac{C}{u_{\tau,p}} = \frac{1}{K}\log(l_\Omega^+) = \frac{1}{K}\log\left(\frac{\mathrm{Re}_{\tau,p}}{\mathrm{Ro}_{\tau,p}}\right), \tag{3}$$

where thesuperscript + denotes normalization by the wall units at the pressure side, and the constant $K \approx \kappa$. Equation (3) is the main conclusion of this paper.

Next, we compare Eq. (3) to data. Mean flow data are extensively available in the literature [22,26–29], and a number of data sets were contributed by the authors of this work [17]. In Figs. 2(a) and 2(b), we compare Eqs. (1) and (3) to data at $\mathrm{Re}_\tau = 180$ and $\mathrm{Ro}_\tau = 0$ to $\mathrm{Ro}_\tau = 130$. For slowly rotating channels, the mean flow will not be very far from the conventional universal logarithmic law of the wall, and the linear scaling Eq. (1) applies to only a limited part of the flow. For rapidly rotating channels, the mean flow follows the linear scaling Eq. (1) in an extended wall-normal distance range from $y = l_\Omega/\kappa$ to a distance above which the flow is laminarlike. In Fig. 2(c), we compare Eq. (3) to the DNS channel at $\mathrm{Re}_\tau = 180$, and in Fig. 2(d), we compare Eq. (3) to the DNS channel at bulk Reynolds numbers Re_b from 5000 to 31 600. The data follow Eq. (3) closely.

These results show that Eq. (3) provides the scaling of C for a wide range of Re_τ and Ro_τ. In the following, we provide arguments for the scaling in Eq. (3) and discuss implications of Eq. (3).

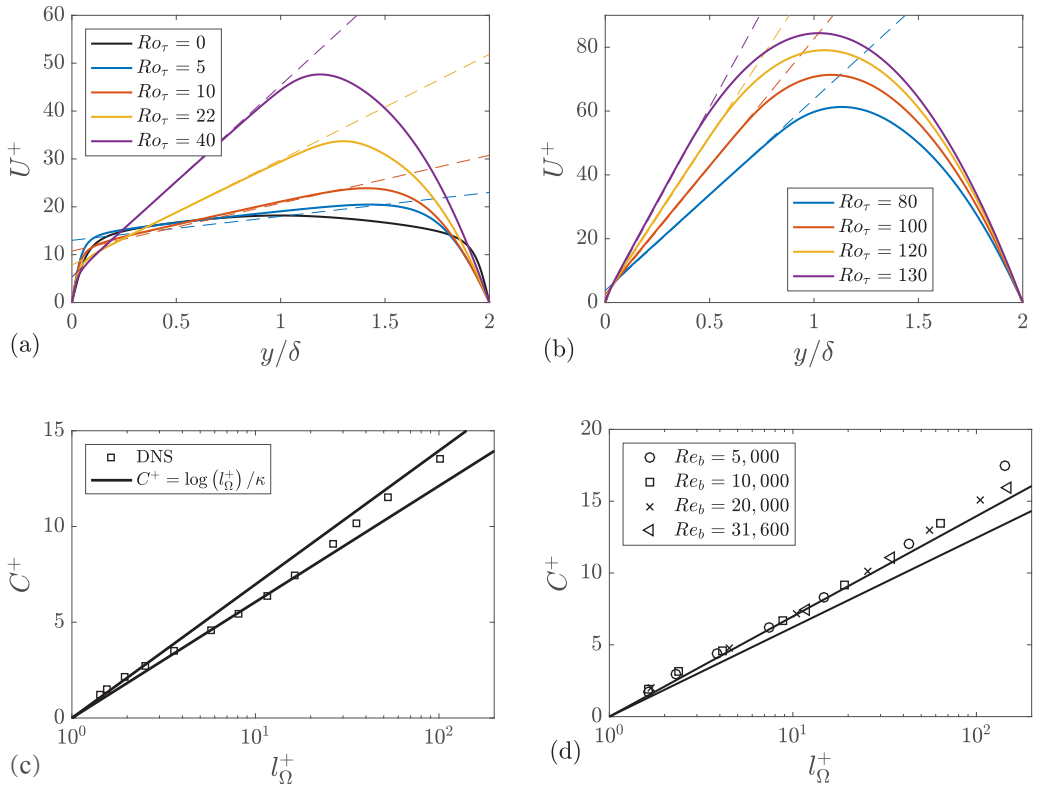

FIG. 2. (a, b) Mean velocities in spanwise rotating channels. Flows are at a constant global friction Reynolds number $\mathrm{Re}_\tau = 180$. Normalization is by the global friction velocity u_τ and the half-channel height, which are kept constant. The flow is laminarlike at the suction side (near $y/\delta = 2$). The dashed lines correspond to Eqs. (1) and (3). Details of the DNS are reported in Ref. [17]. (c, d) The constant C as a function of the rotation length scale l_Ω. Normalization is by wall units at the pressure side. Each data point represents one DNS. (c) Channel flow at $\mathrm{Re}_\tau = 180$ and various rotation numbers. We show lines for two K values, 0.38 and 0.33. (d) Channel flow at five bulk Reynolds numbers and different rotation numbers [26]. The friction Reynolds numbers and the rotation numbers evaluated using quantities at the pressure side are tabulated in Table I. Again, we show predictions for two K values, 0.38 and 0.33. Here, "log" is natural log.

III. A MIXING-LENGTH MODEL

We present a mixing-length-type model which gives rise to the scaling in Eqs. (1) and (3). First, we briefly review Prandtl's mixing-length model.

A. Prandtl's mixing-length hypothesis

Prandtl's mixing-length hypothesis is a classical model of high Reynolds number wall-bounded turbulence in nonrotating frames of Ref. [6]. The model closes the following mean momentum equation [see Ref. [30], Eq. (7.8)]:

$$0 = \frac{d}{dy}\left[-\langle uv\rangle + \nu\frac{dU}{dy}\right] - \frac{1}{\rho}\frac{d\langle P\rangle}{dx}. \tag{4}$$

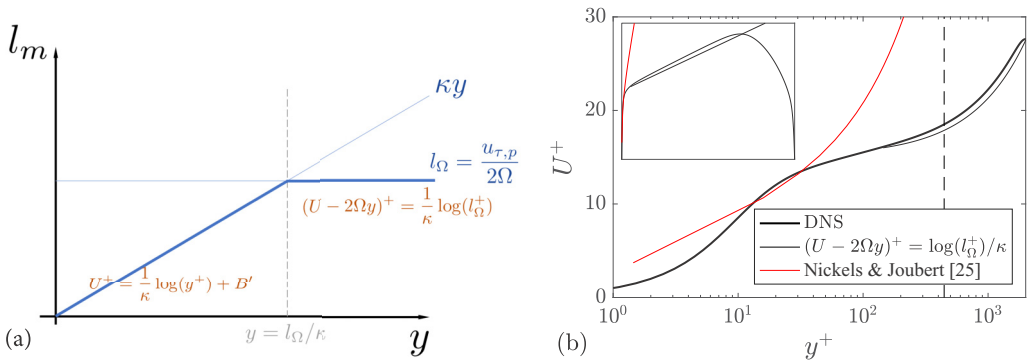

FIG. 3. (a) Mixing length l_m in a spanwise rotating channel. l_m scales as κy up to a wall-normal distance $y = l_\Omega/\kappa$, above which the mixing length stays constant, $l_m = l_\Omega$. (b) Mean flow in a rotating channel at a friction Reynolds number $\mathrm{Re}_\tau = 1213$ and a Rotation number $\mathrm{Ro}_\tau = 11.7$ (bold line) [26]. Normalization is by the wall units at the pressure side. The thin solid line corresponds to the linear law of the wall, i.e., Eqs. (1) and (3), with $K = 0.33$. The dashed line is at $y = l_\Omega/\kappa$. The augmented logarithmic law in Ref. [25] is shown in red and is $U^+ = 1/\kappa \ln y^+ + \beta \mathrm{Rc}(y^+ - 35) + 5$, where $\beta = 9.7$. The inset shows the mean velocity in a linear scale. Here, "log" is natural log.

Prandtl argues that, at high Reynolds numbers, a constant stress layer emerges at wall-normal distances $1 \ll y^+$ and $y \ll \delta$, where the Reynolds shear stress is a constant, i.e.,

$$-\langle uv \rangle = \text{const}, \tag{5}$$

where u and v are the velocity fluctuations in the streamwise and wall-normal directions. Per the mixing-length hypothesis, the Reynolds shear stress may be modeled as the product of an eddy viscosity, ν_T, and the mean velocity gradient, dU/dy, i.e., $-\langle uv \rangle = \nu_T dU/dy$. Prandtl further argued that the eddy viscosity ν_T can be modeled as the product of the square of a mixing length, l_m, and the mean velocity gradient, i.e., $\nu_T = l_m^2 dU/dy$, where the mixing length may be thought of as the size of the eddies at the wall-normal distance y. For a nonrotating channel flow, the mixing length is

$$l_m = \kappa y, \tag{6}$$

and the above arguments give rise to the well-known logarithmic law of the wall in a layer within which the viscous stress is negligible. While this is not the focus of this study, the basic assumption of the attached eddy hypothesis, i.e., the eddies in the logarithmic layer scale as their distances from the wall, follows from Prandtl's mixing-length model.

B. A mixing-length model for flow in spanwise rotating channels

Spanwise rotation leads to a mean Coriolis force in the wall-normal direction, which is balanced by the wall-normal pressure. The mean momentum equation is otherwise unchanged. Equation (4) is the mean flow equation, and Eq. (5) is the equation for the constant stress layer. In order to identify the law of the wall, we need to model the Reynolds shear stress. We follow Prandtl and resort to a mixing-length-type model.

Rotation forces the system at a scale l_Ω. Consequently, rotation limits the mixing length to l_Ω. This length scale competes with the scale of wall-attached eddies, i.e., κy. The end result is a mixing-length scale as shown in Fig. 3(a), where the mixing length l_m increases as κy up to a wall-normal distance $y = l_\Omega/\kappa$, above which the mixing length stays a constant l_Ω, i.e.,

$$l_m = \min[\kappa y, l_\Omega], \quad l_\Omega = \frac{u_{\tau,p}}{2\Omega}. \tag{7}$$

The mixing length is a continuous function of y, hence the transition from $l_m = \kappa y$ to $l_m = l_\Omega$ occurs at $y_c = l_\Omega/\kappa$, where $\kappa y_c = l_\Omega$. Because spanwise rotating channel flow is a different flow than regular channel flow, the constant κ is not necessarily equal to the classical value 0.38 [8].

Invoking the above mixing-length model, the mean flow equation for $y > y_C$ becomes

$$\left(\frac{u_{\tau,p}}{2\Omega}\frac{dU}{dy}\right)^2 = \tau_{w,p}/\rho \equiv u_{\tau,p}^2, \tag{8}$$

where the subscript p indicates quantities evaluated at the pressure side. The above equation gives rise to the linear scaling in Eq. (1). By requiring the mean velocity to be continuous at $y = l_\Omega/\kappa$ and the flow to be laminar at the limit of $l_\Omega^+ = 1$ [17,29], we get Eq. (3), with $K = \kappa$. Hereon, we do not differentiate between K and κ.

It follows from the above discussion that Eq. (3) is a result of velocity continuity at $y = l_\Omega/K$. Hence, for the purpose of Eq. (3), we only require the mixing-length model be valid for $y \leqslant l_\Omega/\kappa$, rather than for all wall-normal distances where $U = 2\Omega y + C$. As $y = l_\Omega/\kappa$ is within the wall-normal distance range that would normally be considered in the logarithmic layer, we could safely say that the mixing-length model here bears the same merit as the mixing-length model for a nonrotating plane channel.

For flows at high Reynolds numbers and high rotation numbers, the mixing-length model suggests a two-layer structure: the mean flow is logarithmic below $y = l_\Omega/\kappa$ and linear above. This is confirmed in Fig. 3(b). In Fig. 3(b), we have also shown the augmented logarithmic law of the wall in Ref. [25]. Since the law of the wall in Ref. [25] is intended for flow in a slowly rotating reference frame (and therefore the comparison shown here is not a fair one), it is expected that it does not capture the mean flow behavior.

While it is not the focus of this work, the mixing-length model suggests that the sizes of the eddies scale as their distance from the wall at distances $y < l_\Omega/\kappa$ and as a constant at distances $y > l_\Omega/\kappa$. However, as the currently available low (to moderate) Reynolds DNS data does not allow us to probe the spatial organization of the linear-layer eddies as, e.g., in Refs. [31–34] for the logarithmic-layer eddies, in this paper, we refrain from making further physical interpretations of the mixing length.

C. Extent of the linear layer and range of model applicability

We discuss at what rotation numbers and Reynolds numbers Eqs. (1) and (3) are valid. The linear layer emerges as the mixing-length transitions from being proportional to the wall-normal distance to a constant. For a nonrotating channel, the mixing length is approximately κy up to a wall-normal distance of $y/\delta \approx 0.2\delta$. In order for the abovementioned transition to take place, the rotation-induced length scale must be such that $l_\Omega \lesssim 0.2\delta$, which leads to $5 \lesssim \mathrm{Ro}_{\tau,p}$. On the other hand, the flow relaminarizes for rotation numbers higher than $\mathrm{Ro}_{\tau,p} = \mathrm{Ro}_\tau \approx \mathrm{Re}_\tau$ (the flow regains symmetry after it relaminarizes). Hence the law of the wall in Eq. (1) is relevant for flows such that

$$5 \lesssim \mathrm{Ro}_{\tau,p}, \quad \mathrm{Ro}_{\tau,p} = \mathrm{Ro}_\tau \lesssim \mathrm{Re}_\tau. \tag{9}$$

Next, we discuss at what wall-normal heights Eqs. (1) and (3) are valid. Per the mixing-length model, the linear law starts at

$$y_s = l_\Omega/\kappa. \tag{10}$$

The end location of the linear law was previously discussed in Ref. [17] and is

$$y_e/\delta = u_{\tau,p}^2/u_\tau^2 - \mathrm{Ro}_\tau/\mathrm{Re}_\tau. \tag{11}$$

Above this height, the flow is laminarlike. Figure 4 shows the mean profiles compensated by the logarithmic scaling. The profiles deviate from the logarithmic scaling at approximately $y_s = l_\Omega/\kappa$, as expected.

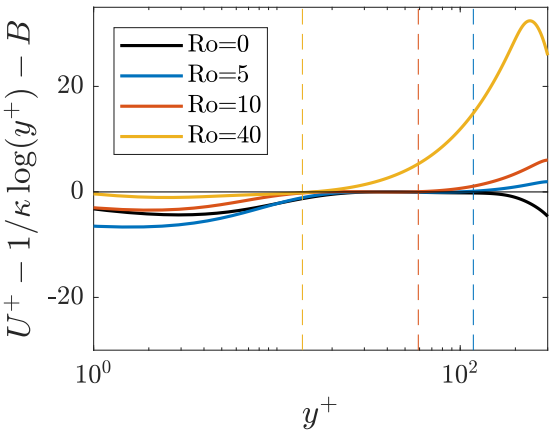

FIG. 4. Mean profiles compensated by the near-wall logarithmic scaling. The data are the same as in Fig. 2(a). The dashed lines correspond to $y_s = l_\Omega/\kappa$ for each case. Per the mixing-length model, the logarithmic scaling ends at y_s and the linear scaling starts at y_s. Here, "log" is natural log.

IV. DISCUSSION

In this section, we discuss a few implications of Eq. (3).

A. Wall modeling

Knowledge of mean flow scaling can be leveraged for large-eddy simulation (LES) wall modeling.

In a wall-modeled LES, the near-wall grid size scales with the local boundary-layer height, and the near-wall turbulence is not resolved by the grid. As a result, the canonical no-slip condition no longer applies, and a wall model will have to be used to supply the LES equations with a proper wall boundary condition [11]. A commonly used approach is to invoke the law of the wall and relate the wall shear stress to the near-wall LES velocity [35–39]. For flows in spanwise rotating channels, the conventional universal logarithmic law of the wall loses partly its predictive power, and Eqs. (1) and (3) will need to be employed. It follows that, for a rapidly rotating channel, with $l_\Omega/\kappa < \Delta$, the wall shear stress in a spanwise rotating channel can be modeled as

$$\tau_{w,p}/\rho = \left[\frac{\kappa(U - 2\Omega y)}{\log(l_\Omega^+)}\right]^2. \tag{12}$$

Here, Δ is the grid spacing in the wall-normal direction. We test Eq. (12) by comparing the measured wall shear stresses to the right-hand side of Eq. (12) in Fig. 5, using data from Ref. [26]. We use data at three representative rotation numbers, $\mathrm{Ro}_\tau = 11.7$, 34.6, and 67.4, and one bulk Reynolds number, $\mathrm{Re}_b = 31\,600$. The computed values are fairly close to the DNS values if using velocity information at distances $y/\delta \gtrsim 0.1$, which is typically where the first off-wall grid is in wall-modeled LES.

B. Friction Reynolds number and bulk Reynolds number

The mean flow information can be used to compute the friction Reynolds number from the bulk Reynolds number and vice versa.

Following the above discussion, the mean velocity in a spanwise rotating channel follows Eqs. (1) and (3) near the pressure side and is laminarlike near the suction side. We neglect the viscous sublayer and the logarithmic layer at the pressure side, both of which occupy only a small part of

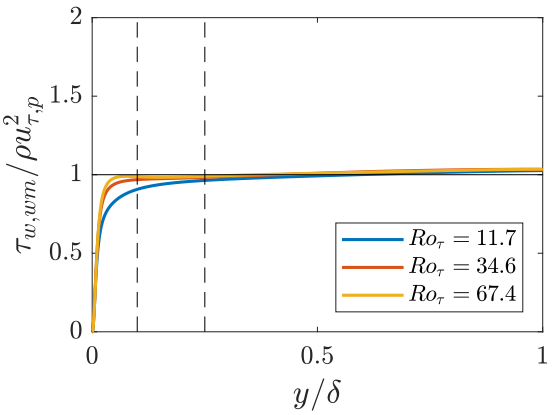

FIG. 5. $\tau_{w,wm}$ is the wall shear stress computed according to Eq. (12). We use velocity data at three representative rotation numbers, $\mathrm{Ro}_\tau = 11.7$, 34.6, and 67.4, and one bulk Reynolds number, $\mathrm{Re}_b = 31\,600$ [26]. The dashed lines are at $y/\delta = 0.1$ and 0.25. In a wall-modeled LES, the first grid point typically locates at $y \approx O(0.1\delta)$ [40], and the third grid point at $y \approx O(0.25\delta)$ [36].

the domain at high rotation numbers. We assume that the mean flow follows Eq. (1) from $y = 0$ to $y_e/\delta = u_{\tau,p}^2/u_\tau^2 - \mathrm{Ro}_\tau/\mathrm{Re}_\tau$, above which the mean flow is parabolic:

$$U = a(y - 2\delta)^2 + b(y - 2\delta), \tag{13}$$

where $U = 0$ at $y = 2\delta$ per the no-slip condition. Define $u_{\tau,s}$ to be the friction velocity at the suction side; it follows that $-\nu dU/dy|_{y=2\delta} = u_{\tau,s}^2$ and

$$b = -\frac{u_{\tau,s}^2}{\nu}. \tag{14}$$

Because the flow is laminarlike at the suction side, the streamwise momentum equation reduces to

$$-\frac{1}{\rho}\frac{dP}{dx} + \nu\frac{d^2U}{dy^2} = 0, \tag{15}$$

which leads to

$$a = \frac{1}{2\nu}\frac{1}{\rho}\frac{dP}{dx}. \tag{16}$$

If we enforce the following constraints: first, the mean momentum conservation, i.e.,

$$u_{\tau,s}^2 + u_{\tau,p}^2 = 2u_\tau^2; \tag{17}$$

second, the velocity continuity at y_e, i.e.,

$$2\Omega y_e + C = a(y_e - 2\delta)^2 + b(y_e - 2\delta); \tag{18}$$

and third, the definition of the friction velocity, i.e.,

$$u_\tau^2 = -\frac{1}{\rho}\frac{dP}{dx}\delta, \tag{19}$$

depending on if the friction Reynolds number or the bulk Reynolds number is known, we can compute the bulk Reynolds number (bulk velocity) from the friction Reynolds number (friction velocity) from Eqs. (13)–(19) and vice versa. The equations are implicit, but the solution converges within a few iterations (if using the built-in fsolve function in MATLAB). In Fig. 6(a), we compare the model-predicted bulk velocities to DNS for flows at a fixed friction Reynolds number, i.e.,

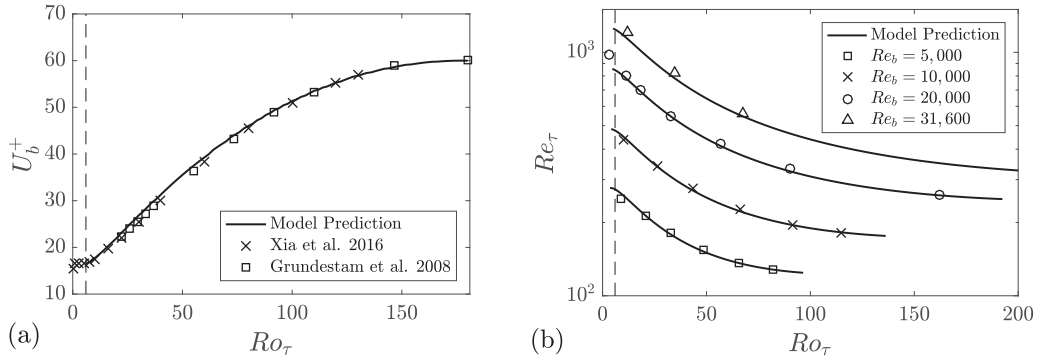

FIG. 6. (a) Predicted bulk velocities (lines) and DNS data (symbols) as functions of the global rotation number for flows at a fixed friction Reynolds number $\mathrm{Re}_\tau = 180$. The dashed line is at $\mathrm{Ro}_\tau = 6$ ($\mathrm{Ro}_{\tau,p} \approx 5$), above which we consider as rapid rotation. (b) Predicted global friction Reynolds numbers (line) and DNS data (symbols) as functions of the global rotation number for flows at a few fixed bulk Reynolds numbers. The dashed line is at $\mathrm{Ro}_\tau = 6$ ($\mathrm{Ro}_{\tau,p} \approx 5$).

$\mathrm{Re}_\tau = 180$, and in Fig. 6(b), we compare the model-predicted friction Reynolds numbers to DNS for flows at a few fixed bulk Reynolds numbers. The data follow the model predictions closely.

C. The physics behind a constant mixing length

Per the mixing-length model, rotation forces the system at a constant length scale l_Ω, leading to a constant mixing length. A constant mixing length was previously used to model the wake region of a wall-bounded flow [30], where the flow is conventionally regarded as not being forced at any scale. In the light of the recent works [41,42], flow in the wake layer is affected by the nonturbulent freestream, which "forces" the flow at a constant length scale $O(\delta)$. Considering the present mixing-length model and these recent works, we think the physics about the constant mixing length in the wake layer may need to be revised.

D. Slowly rotating channels

The mixing-length model gives rise to a logarithmic mean flow for $y < l_\Omega/\kappa$ and a linear mean flow for $y > l_\Omega/\kappa$. By requiring the mean flow to be continuous at $y = l_\Omega/\kappa$, we get Eq. (3). For rapidly rotating channels at a high Reynolds number, i.e., for $y = l_\Omega/\kappa$ in the constant stress layer, the above procedure works well (see Fig. 7, the purple line). However, for slowly rotating channels, where $l_\Omega = u_{\tau,p}/2\Omega$ is comparable to δ and $y = l_\Omega/\kappa$ is in the wake layer, the above procedure may not work well (see Fig. 7, the yellow line). As sketched in Fig. 7, positive deviations from Eq. (3) are expected at small Ro_τ. This expectation bears out in Fig. 8, where we show the compensated plots of the lines in Figs. 2(c) and 2(d).

In addition to deviations at low rotation numbers, i.e., at high l_Ω values, deviations are also found at high rotation numbers, i.e., at low l_Ω values. This limit of very rapidly rotating channels is discussed in Ref. [17], and for very rapidly rotating channels such that $l_\Omega^+ = 1$, $C^+ = 0$ and Eq. (3) must hold. Hence deviations from Eq. (3) at fast rotation may just be a result of uncertainties in the data and our postprocessing. (Note that the grid resolutions in Refs. [17,26] are different.)

E. Further remarks on the mixing-length model

The conventional logarithmic law of the wall can be obtained from the mixing-length model [6], the attached eddy hypothesis [43], dimensional analysis [30], and analytical analysis of the turbulent kinetic energy equation [44]. Likewise, the mixing-length model in Sec. III is, by no means, the only

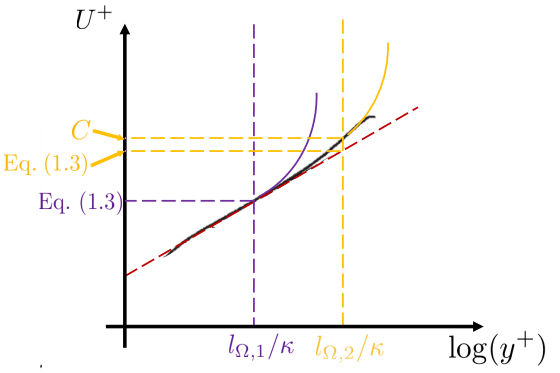

FIG. 7. A sketch of the mean flows in a rapidly rotating channel (the purple line) and a slowly rotating channel (the yellow line). Here, "log" is natural log.

model that gives rise to $U = 2\Omega y + C$. Zhang *et al.* [45] showed that by neglecting the viscous force and the pressure force and tracking a fluid parcel, i.e.,

$$\frac{du}{dt} = 2\Omega \frac{dy}{dt}, \tag{20}$$

one can conclude that the mean flow in a two-dimensional three-component spanwise rotating channel is $U = 2\Omega y + C$, shedding light on the mean flow behavior in a three-dimensional spanwise rotating channel. Brethouwer [26] examined the Reynolds stress equations and concluded from his DNSs that at wall-normal distances where $U = 2\Omega y + C$, the production term balances the Coriolis force term, i.e.,

$$-\langle u'v' \rangle \frac{dU}{dy} + 2\Omega \langle u'v' \rangle \approx 0, \tag{21}$$

which directly leads to $U = 2\Omega y + C$. Nakabayashi and Kitoh [19] conducted dimensional analysis and argued that rotation dominates in the core region and therefore

$$\frac{dU}{dy} = A\Omega, \tag{22}$$

which also leads to $dU/dy \sim \Omega$. Nonetheless, the above works did not discuss the scaling for C, which is the focus of this work.

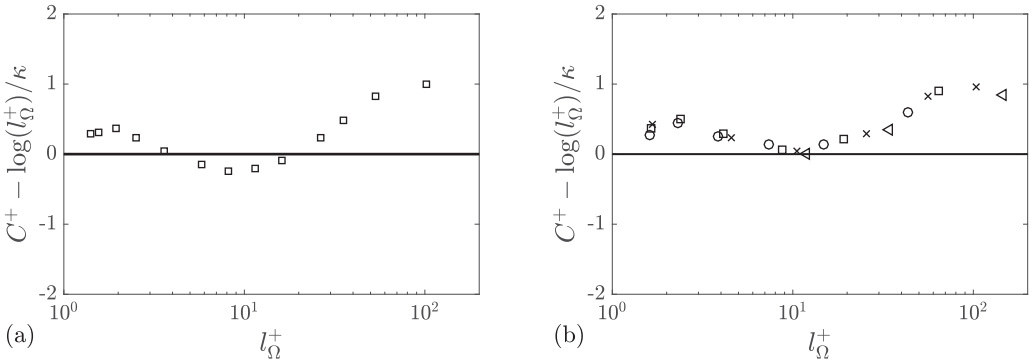

FIG. 8. Compensated plots. The symbols are the same as those in Figs. 2(c) and 2(d). Here, "log" is natural log.

That being said, among the models and theories that give rise to the conventional logarithmic law of the wall, Prandtl's mixing-length model sees the most use in turbulence modeling. LES wall models [10,11], Reynolds averaged Navier Stokes (RANS) models [46,47], and canopy models [38,48] all rely on the mixing-length model (to some extent). Hence, in this paper, we have focused our discussion on the mixing-length model and its predictions.

V. CONCLUSIONS

Since the early work of Johnston *et al.* [18], the mean flow scaling in a spanwise rotating channel has received much attention. While it is well known that $U = 2\Omega y + C$, the scaling of C as a function of the Reynolds number and the rotation number has been an open question. In this work, we show that

$$C^+ = \frac{1}{K}\log(l_\Omega^+) = \frac{1}{K}\log\left(\frac{\mathrm{Re}_{\tau,p}}{\mathrm{Ro}_{\tau,p}}\right).$$

Here, the superscript + represents normalization using wall units at the pressure side, K is a constant whose numeric value is very close to the von Karman constant, Ω is the rotation speed, and log is natural log.

In addition to confirming the above scaling in data, we discussed a few implications of the mean flow scaling. First, the mean flow information can be used for LES wall modeling of spanwise rotating channels [49]. Second, the knowledge of the mean flow could be used to relate the bulk Reynolds number and the friction Reynolds number. Third, we argue that a constant mixing length suggests "forcing" at a constant length scale. Last, it is worth mentioning that the identified mean flow scaling may also be relevant to Taylor-Couette flow [50,51], which is left for future investigation.

ACKNOWLEDGMENTS

X.Y. acknowledges the funding support to the CTR summer program, which made it possible for scientists from five different institutions to collaborate. Z.-H.X. thanks S. Chen for many valuable comments and the National Natural Science Foundation of China (Grants No. 11772297 and No. 11822208) for financial support. X.Y. would like to thanks P. Moin and U. Piomelli for insightful comments and M.-W. Ge for editing the text. J.Y. thanks U. Piomelli and W. Wu for sharing the high Reynolds number DNS data.

[1] S. Jakirlic, K. Hanjalic, and C. Tropea, Modeling rotating and swirling turbulent flows: A perpetual challenge, AIAA J. **40**, 1984 (2002).

[2] P. E. Smirnov and F. R. Menter, Sensitization of the SST turbulence model to rotation and curvature by applying the Spalart–Shur correction term, J. Turbomach. **131**, 041010 (2009).

[3] S. K. Arolla and P. A. Durbin, Modeling rotation and curvature effects within scalar eddy viscosity model framework, Int. J. Heat Fluid Flow **39**, 78 (2013).

[4] A. S. Hsieh, S. Biringen, and A. Kucala, Simulation of rotating channel flow with heat transfer: Evaluation of closure models, J. Turbomach. **138**, 111009 (2016).

[5] H. Choi and P. Moin, Grid-point requirements for large eddy simulation: Chapman's estimates revisited, Phys. Fluids **24**, 011702 (2012).

[6] L. Prandtl, Bericht uber untersuchungen zur ausgebildeten turbulenz, Z. Angew. Math. Mech. **5**, 136 (1925).

[7] T. Von Kármán, Mechanische aehnlichkeit und turbulenz, in *Proceedings of the Third International Congress for Applied Mechanics*, edited by C. W. Oseen and W. Weibull (1930), Vol. 1, pp. 79–93 (in German).

[8] I. Marusic, J. P. Monty, M. Hultmark, and A. J. Smits, On the logarithmic region in wall turbulence, J. Fluid Mech. **716**, R3 (2013).
[9] H. M. Nagib and K. A. Chauhan, Variations of von Kármán coefficient in canonical flows, Phys. Fluids **20**, 101518 (2008).
[10] U. Piomelli and E. Balaras, Wall-layer models for large-eddy simulations, Annu. Rev. Fluid Mech. **34**, 349 (2002).
[11] S. T. Bose and G. I. Park, Wall-modeled large-eddy simulation for complex turbulent flows, Annu. Rev. Fluid Mech. **50**, 535 (2018).
[12] X. I. A. Yang and C. Meneveau, Recycling inflow method for simulations of spatially evolving turbulent boundary layers over rough surfaces, J. Turbul. **17**, 75 (2016).
[13] B. E. Launder, D. P. Tselepidakis, and B. A. Younis, A second-moment closure study of rotating channel flow, J. Fluid Mech. **183**, 63 (1987).
[14] F. Hamba, The mechanism of zero mean absolute vorticity state in rotating channel flow, Phys. Fluids **18**, 125104 (2006).
[15] O. Grundestam, S. Wallin, and A. V. Johansson, A priori evaluations and least-squares optimizations of turbulence models for fully developed rotating turbulent channel flow, Eur. J. Mech. B: Fluids **27**, 75 (2008).
[16] R. Kristoffersen and H. I. Andersson, Direct simulations of low-Reynolds-number turbulent flow in a rotating channel, J. Fluid Mech. **256**, 163 (1993).
[17] Z. Xia, Y. Shi, and S. Chen, Direct numerical simulation of turbulent channel flow with spanwise rotation, J. Fluid Mech. **788**, 42 (2016).
[18] J. P. Johnston, R. M. Halleent, and D. K. Lezius, Effects of spanwise rotation on the structure of two-dimensional fully developed turbulent channel flow, J. Fluid Mech. **56**, 533 (1972).
[19] K. Nakabayashi and O. Kitoh, Low Reynolds number fully developed two-dimensional turbulent channel flow with system rotation, J. Fluid Mech. **315**, 1 (1996).
[20] Y. Maciel, D. Picard, G. Yan, C. Gleyzes, and G. Dumas, Fully developed turbulent channel flow subject to system rotation, in *Proceedings of the 33rd AIAA Fluid Dynamics Conference and Exhibit* (2003), p. 4153.
[21] K. Nakabayashi and O. Kitoh, Turbulence characteristics of two-dimensional channel flow with system rotation, J. Fluid Mech. **528**, 355 (2005).
[22] Y.-T. Yang and J.-Z. Wu, Channel turbulence with spanwise rotation studied using helical wave decomposition, J. Fluid Mech. **692**, 137 (2012).
[23] Y.-J. Dai, W.-X. Huang, and C.-X. Xu, Effects of Taylor-Görtler vortices on turbulent flows in a spanwise-rotating channel, Phys. Fluids **28**, 115104 (2016).
[24] A. Hsieh and S. Biringen, The minimal flow unit in complex turbulent flows, Phys. Fluids **28**, 125102 (2016).
[25] T. B. Nickels and P. N. Joubert, The mean velocity profile of turbulent boundary layers with system rotation, J. Fluid Mech. **408**, 323 (2000).
[26] G. Brethouwer, Statistics and structure of spanwise rotating turbulent channel flow at moderate Reynolds numbers, J. Fluid Mech. **828**, 424 (2017).
[27] W. Wu, U. Piomelli, and J. Yuan, Turbulence statistics in rotating channel flows with rough walls, Int. J. Heat Fluid Flow **80**, 108467 (2019).
[28] E. Lamballais, M. Lesieur, and O. Métais, Effects of spanwise rotation on the vorticity stretching in transitional and turbulent channel flow, Int. J. Heat Fluid Flow **17**, 324 (1996).
[29] O. Grundestam, S. Wallin, and A. V. Johansson, Direct numerical simulations of rotating turbulent channel flow, J. Fluid Mech. **598**, 177 (2008).
[30] S. B. Pope, *Turbulent Flows* (Cambridge University, Cambridge, England, 2001).
[31] X. I. A. Yang, I. Marusic, and C. Meneveau, Hierarchical random additive process and logarithmic scaling of generalized high order, two-point correlations in turbulent boundary layer flow, Phys. Rev. Fluids **1**, 024402 (2016).
[32] X. I. A. Yang and M. Abkar, A hierarchical random additive model for passive scalars in wall-bounded flows at high Reynolds numbers, J. Fluid Mech. **842**, 354 (2018).

[33] F. Eich, C. M. de Silva, I. Marusic, and C. J. Kähler, Towards an improved spatial representation of a boundary layer from the attached eddy model, Phys. Rev. Fluids **5**, 034601 (2020).
[34] C. M. de Silva, J. D. Woodcock, N. Hutchins, and I. Marusic, Influence of spatial exclusion on the statistical behavior of attached eddies, Phys. Rev. Fluids **1**, 022401 (2016).
[35] U. Schumann, Subgrid scale model for finite difference simulations of turbulent flows in plane channels and annuli, J. Comput. Phys. **18**, 376 (1975).
[36] S. Kawai and J. Larsson, Wall-modeling in large eddy simulation: Length scales, grid resolution, and accuracy, Phys. Fluids **24**, 015105 (2012).
[37] X. I. A. Yang, J. Sadique, R. Mittal, and C. Meneveau, Integral wall model for large eddy simulations of wall-bounded turbulent flows, Phys. Fluids **27**, 025112 (2015).
[38] X. I. A. Yang, J. Sadique, R. Mittal, and C. Meneveau, Exponential roughness layer and analytical model for turbulent boundary layer flow over rectangular-prism roughness elements, J. Fluid Mech. **789**, 127 (2016).
[39] G. I. Park and P. Moin, An improved dynamic non-equilibrium wall-model for large eddy simulation, Phys. Fluids **26**, 37 (2014).
[40] X. I. A. Yang, G. I. Park, and P. Moin, Log-layer mismatch and modeling of the fluctuating wall stress in wall-modeled large-eddy simulations, Phys. Rev. Fluids **2**, 104601 (2017).
[41] Y. Kwon, The quiescent core of turbulent channel and pipe flows, Ph.D. thesis, University of Melbourne, 2016.
[42] D. Krug, J. Philip, and I. Marusic, Revisiting the law of the wake in wall turbulence, J. Fluid Mech. **811**, 421 (2017).
[43] A. A. Townsend, *The Structure of Turbulent Shear Flow* (Cambridge University, Cambridge, England, 1976).
[44] J. Jiménez, Cascades in wall-bounded turbulence, Annu. Rev. Fluid Mech. **44**, 27 (2012).
[45] S. Zhang, Z. Xia, Y. Shi, and S. Chen, A two-dimensional-three-component model for spanwise rotating plane Poiseuille flow, J. Fluid Mech. **880**, 478 (2019).
[46] F. R. Menter, Review of the shear-stress transport turbulence model experience from an industrial perspective, Int. J. Comput. Fluid Dyn. **23**, 305 (2009).
[47] G. L. Mellor and T. Yamada, Development of a turbulence closure model for geophysical fluid problems, Rev. Geophys. **20**, 851 (1982).
[48] O. Coceal and S. E. Belcher, A canopy model of mean winds through urban areas, Q. J. R. Meteorol. Soc. **130**, 1349 (2004).
[49] X. L. D. Huang, X. I. A. Yang, and R. F. Kunz, Wall-modeled large-eddy simulations of spanwise rotating turbulent channels comparing a physics-based approach and a data-based approach, Phys. Fluids **31**, 125105 (2019).
[50] S. Grossmann, D. Lohse, and C. Sun, High-Reynolds number Taylor-Couette turbulence, Annu. Rev. Fluid Mech. **48**, 53 (2016).
[51] X. Zhu, R. A. Verschoof, D. Bakhuis, S. G. Huisman, R. Verzicco, C. Sun, and D. Lohse, Wall roughness induces asymptotic ultimate turbulence, Nat. Phys. **14**, 417 (2018).